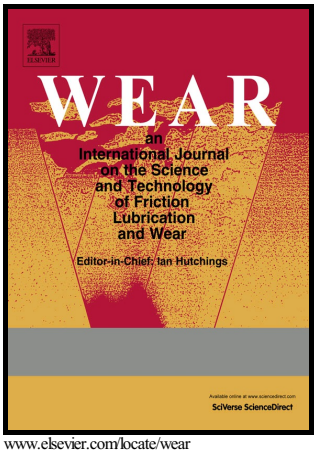

www.elsevier.com/locate/wear

The effect of non-uniform train speed distribution on rail corrugation growth in curves/corners

P.A. Meehan, R.D. Batten, P.A. Bellette

PII: S0043-1648(16)30085-0
DOI: http://dx.doi.org/10.1016/j.wear.2016.05.009
Reference: WEA101686

To appear in: *Wear*

Received date: 30 September 2015
Revised date: 5 May 2016
Accepted date: 10 May 2016

Cite this article as: P.A. Meehan, R.D. Batten and P.A. Bellette, The effect of non-uniform train speed distribution on rail corrugation growth in curves/corners *Wear,* http://dx.doi.org/10.1016/j.wear.2016.05.009

The effect of non-uniform train speed distribution on rail corrugation growth in curves/corners

P.A. Meehan[a] , R.D. Batten[a] and P.A. Bellette[a]

[a] School of Mechanical and Mining Engineering, University of Queensland & Rail CRC, Brisbane, QLD 4072, Australia
Email: meehan@uq.edu.au

ABSTRACT

Rail corrugation is a significant problem in railway engineering, manifesting as an oscillatory wear pattern on the rail head. These profile variations induce unwanted vibrations, excessive noise and other associated problems. Constant train speed for consecutive train passes has been shown to accelerate corrugation growth while widening the probabilistic speed distribution can be shown to mitigate the phenomena. This paper extends this research by investigating the effect of non-uniformity (or asymmetry) in speed distribution on corrugation growth on curved track/corners. To this end, an efficient corrugation growth prediction model is further developed to include quasistatic bogie cornering dynamics and investigated under non-uniform speed distribution conditions. The results indicate that under typical cornering conditions, the rate of corrugation growth is increased (or decreased) when the mean or skewness of the distributed set of passing speeds is biased to higher (or lower) speeds. In particular, for the conditions investigated, controlling (or not controlling) skewness could achieve a further 12% (or -20%) in corrugation growth rate reduction from a nominal 41% reduction due to symmetric speed variation. Hence, non-uniform speed distribution could cause up to a 50% reduction in predicted effectiveness of widened speed distribution control to reduce corrugation growth rate.

Keywords: rail corrugation; rolling contact wear; vibrations; wear modelling, non-uniform speed distribution

1. INTRODUCTION

Wear-type rail corrugation is a dynamic wheel-rail contact phenomena that manifests as a periodic wear pattern on rail heads. It is a significant problem in railways worldwide [1] that grows over many train passages, causing unwanted vibrations, excessive noise and other associated problems. *Figure 1* shows a corrugation profile after approximately 9 months of passenger rail traffic. Recent studies have shown that uniformity in train passing speed accelerates corrugation growth on straight track and conversely, widening the probabilistic train passing speed distribution can be used as a mitigation tool. The dominant mitigating mechanism is that different vehicle speeds lead to different wavelengths and positions of periodic wear along the track and therefore cancellation of corrugation growth.

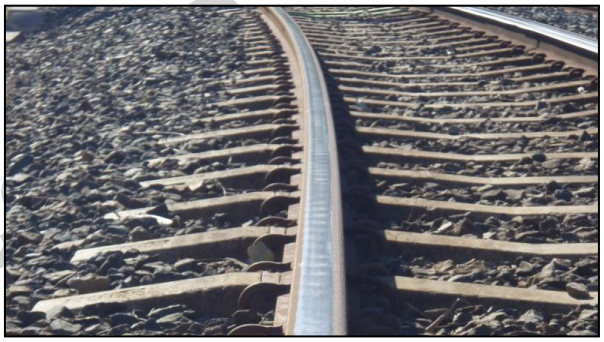

Figure 1 – 9-month-old corrugated rail profile

Wear-type rail corrugation is caused by vehicle vibrations interacting with oscillatory contact conditions between the wheel and rail, resulting in a periodic variance in frictional power between the two running surfaces. This in turn differentially wears the surface of the rail, resulting in a ripple pattern on the rail head. This corrugated profile re-excites the wheel-rail contact and vehicle on subsequent wheel passages, at a similar vibration frequency if the speed is similar, which accelerates the growth process [2]. The primary cure for corrugations at present is expensive reprofiling of the rail by grinding. To better understand this problem, a number of models to simulate the rail corrugation growth process have been developed. Simplified analytical corrugation prediction models have shown the capacity to predict dominant frequencies and amplitudes in dynamic normal force oscillation and subsequently, associated corrugation growth rates [2-6]. More complex three dimensional numerical models can provide more fidelity but are computationally expensive, making effective analysis of speed distribution effects over many vehicle passes difficult. However, simplifications in modelling based on identifying the dominant interactions may be used to provide efficient analysis such as that developed in [7]. A variety of control techniques have also been proposed and developed to mitigate rail corrugation growth. Most have proven unreliable under varying conditions (see reviews of [1, 8]). However the application of friction modifiers [22,23] for reducing the occurrence of rail corrugations has been relatively successful by changing the friction coefficient and stick-slip behaviour in the contact. Alternatively, recent studies have shown that widening the probabilistic passing speed distribution over a section of rail can be an effective corrugation mitigation tool [7, 9, 10], although environmental effects may swamp performance in the field [24]. Often though, the variance of train speed approved by rail operators will be limited in order to meet existing timetables. For this reason, the

amount of increase of train passing speed standard deviation may be limited, so alternative methods of controlling the train passing speed distribution for mitigating corrugation growth is of interest.

This paper aims to predict and quantify the effects of using a non-uniform speed distribution on the corrugation growth rate under curving/cornering conditions. In particular, asymmetric speed distribution parameters are defined and the additional benefits of asymmetry in corrugation control under a range of bogie cornering speeds are investigated. This was achieved by integrating triangular speed distributions of varying skewness to quantify its effects on the growth rate of the dominant wavelength of corrugation formation. The main contributions of this paper are an enhancement and validation of an efficient corrugation growth model to include bogie-wagon cornering dynamics and quantification of the effect of non-uniform speed distribution on rail corrugation growth in cornering/curved track conditions.

To this end, a modified frequency domain corrugation model is first presented as a sequence of transfer functions and combined with a variable speed input to create a new, efficient corrugation growth model for cornering/curving conditions. It is noted that the modelling is made as simple as possible to enable efficient calculation of a distribution of train pass velocities while encapsulating the dominant dynamic behaviour. Subsequently, a method of integrating the corrugation growth function with a series of asymmetric triangular speed distributions is provided. The direct effects of nominal speed on corrugation growth on both rails in cornering is then determined and discussed. Cornering/curving results of traction and bogie yaw angle were benchmarked against a linearized cornering model presented in Wickens [16] and corrugation growth rate was benchmarked against modelling from Daniel et.al. [19]. Finally, the effect of non-uniform speed distribution on corrugation growth in cornering is quantified under a case study.

2. THEORETICAL MODELLING

Corrugation modelling consists of four basic components shown in *Figure 2*: (I) vibrational dynamics of the train and track causing oscillating contact forces, (II) contact variations in the interface between the rail head and wheel, (III) material removal from the rail head due to variation in frictional power at the contact interface, and (IV) transient dynamic effects between successive wheel passes due to a finite pass delay. Component IV isn't considered in the present paper but its effects are detailed in [11].

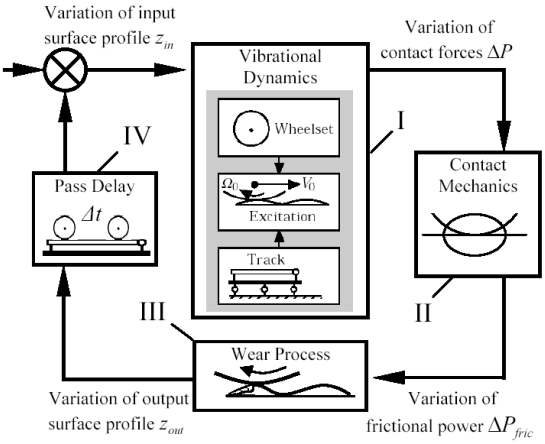

Figure 2 – Corrugation modelling block diagram

The following subsections outline details of the components in *Figure 2* used to derive a corrugation growth expression for a bogie in cornering under varying speed conditions. In this case, the corrugation mechanism is based on the field and modelled behaviour identified in [7] whereby cornering corrugations were shown to be associated with dynamic normal forcing of the wheel/rail contact inducing high amplitudes of varying lateral slip. This behaviour was validated using a more complex 3D model and field measurements where vertical dynamics was shown to dominate because the high effective lateral contact damping is found to minimise the effect of the lateral dynamics (see Appendix in [7]). Hence rail corrugation growth caused by wheelset torsional oscillation modes is not considered in this paper. In addition, in order to develop an efficient corrugation growth model, the vehicle-track dynamics is modelled using a rigid wheelset and a finite number of modes in the frequency range of curving corrugations of interest (ie typically 50 – 500Hz). This approach was validated with field measurements in [17]. However this assumption could be relaxed by the use of measured receptances if desired. Also transient and nonlinear geometric contact mechanics associated with short pitch corrugations, that typically do not occur in curves, are also ignored.

2.1 Vibrational dynamics (I)

In the presence of high lateral contact damping experienced at creep conditions below critical, vibrational dynamics in cornering are dominated by vertical rail and wheel responses to existing profile height variations [7]. In particular, in this case the mechanism of corrugation growth is dominated by lateral traction variations, predominantly excited by vertical vibrations due to high lateral contact damping. Further details, validated by field measurements are provided in [7]. Hence, lateral dynamics are neglected in predicting corrugation growth in this paper. Under these conditions, referring to *Figure 2*(I), the normal contact force variation, ΔP, resulting from an input surface profile height variance Z_n, may be adequately expressed using the following receptance based equation [13],

$$\Delta P / Z_n(\omega) = k_c / [1 + k_c \left(R_{rv}(\omega) + R_{wv}(\omega) \right)] , \qquad (1)$$

where R_{rv} and R_{wv} are the vertical rail and wheel receptance functions of frequency, ω, and k_c is the contact stiffness, predetermined by the steady state normal force [13]. A five mode track model was utilised to model a typical vertical track receptance (see Appendix A) and the wheel receptance was assumed to be that of the unsprung mass.

2.2 Contact mechanics (II)

The variation in normal contact forces causes a variation in frictional power due to the contact mechanics of a bogie negotiating a curve (see *Figure 2*,II). In order to evaluate the frictional power variance due to contact force variances, the steady state wheel slip and associated sensitivity to normal force variation must be calculated for each wheel of a bogie in cornering. The traction-to-slip relation can be calculated based on a combination of the work of Shen *et. al.*, (1993) [14] and Polach (2003) [15]. The contribution of longitudinal traction and wear to corrugation growth is neglected in this analysis based on the field and modelling analysis in [7]. In addition, the present model focusses on curving corrugations with a wavelength well above short pitch corrugations. Under these assumptions, efficient quasistatic traction-creep equations may be utilised based on an empirical curve fitted to experimental data for traction ratio variance with slip ratio, ξ_i, normalized to a critical slip ratio, ξ_c in the form,

$$Q_i(\xi,V)=\begin{cases}\mu_i(\xi)P_i(V)\left(1-\left(1-\xi_i/\xi_c\right)^3\right) & \xi_i/\xi_c<1\\ \mu_i(\xi)P_i(V) & \xi_i/\xi_c\geq 1\end{cases}. \tag{2}$$

$$\mu_i(\xi)=\mu_0\left[(1-A)e^{-B\xi_i/\xi_c}+A\right], \tag{3}$$

$$A=\mu_\infty/\mu_0 \tag{4}$$

The critical slip ratio, ξ_c, is a function of the contact patch dimensions of major and minor semi axes, a and b, as well as normal force, P_i, shear modulus, G, effective friction coefficient, μ_i, a Kalker coefficient, C_{22}, for lateral traction, Poisson's ratio, ν, and Young's modulus, E, such that,

$$\xi_c=\frac{3\mu_i P_i}{C_{22}Gab},\ a,b=\sqrt[3]{\left(\frac{R'}{R''}\right)^{\pm 1}\frac{3P_i\sqrt{R'R''}(1-\nu^2)}{4E}F_1\left(\frac{R'}{R''}\right)} \tag{5}$$

$$a,b=\sqrt[3]{\left(\frac{R'}{R''}\right)^{\pm 1}\frac{3P_i\sqrt{R'R''}(1-\nu^2)}{4E}F_1\left(\frac{R'}{R''}\right)} \tag{6,7}$$

where F_1 is a scaling function due to the contact patch eccentricity detailed in [13]. The modelled contact geometry between the wheel and rail is assumed to be a Hertzian ellipse governed by equations (6) and (7) where longitudinal and lateral relative radii, *R'* and *R''*, describe the local curvature at the contact of the wheel-rail profiles. In order to calculate lateral traction forces, Q_i, of the wheels, the traction ratio and the steady state cornering normal forces on the high and low rails, P_i, are required. These were derived via a force balance calculation on the cornering vehicle to find the steady state wagon roll and subsequently the normal reaction forces through the rails.

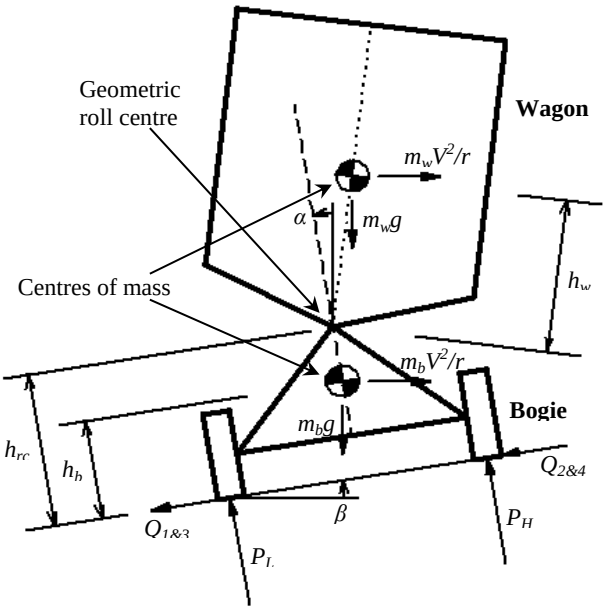

Figure 3 – Wagon roll, rail reaction forces and associated train parameters in curving/cornering.

Referring to *Figure 3*, the geometric roll centre is defined by the suspension setup. The height of the geometric roll centre and bogie centroid, normal to the track are given by h_{rc} and h_b respectively and h_w indicates the distance of the wagon centroid from the geometric roll centre. The wagon and bogie have masses of m_w and m_b respectively. The steady state normal forces on the low and high rails are P_L and P_H and the angle of cant is defined by β. Centrifugal tipping torques caused by navigating a corner of radius, r, at a constant velocity, V, and gravitational forces above the roll centre are balanced by the rolling stiffness, k_{roll}, combined with the angular deflection, α such that,

$$\alpha(V)=[g\cdot h_w\cdot\beta-V^2\cdot h_w/r]/[g\cdot h_w-k_{roll}/m_w]. \tag{8}$$

With the roll angle of a cornering wagon defined, the steady state normal forces on the high and low rails, P_H and P_L, can be calculated via global moment balance about the contact points on opposing rails as functions of wagon and bogie properties, track width, w, train speed, corner radius and total train mass, m_t, as,

$$P_L(V)=\left(\frac{m_tg}{2}-\frac{(m_wh_{rc}+m_bh_b)V^2}{rw}\right)\cos(\beta)+\left(\frac{m_tV^2}{2r}+\frac{(m_wh_{rc}+m_bh_b)g}{w}\right)\sin(\beta)-\frac{k_{roll}\alpha(V)}{w}, \tag{9}$$

$$P_H(V) = \left(\frac{m_t g}{2} + \frac{(m_w h_{rc} + m_b h_b)V^2}{rw}\right)\cos(\beta) + \left(\frac{m_t V^2}{2r} - \frac{(m_w h_{rc} + m_b h_b)g}{w}\right)\sin(\beta) + \frac{k_{roll}\alpha(V)}{w}, \quad (10)$$

The normal forces on the high and low rails are dominated by the first terms of the respective equations. This consists of half the weight of the train on each rail with a transfer of weight due to an induced centrifugal tipping torque, which increases with speed. The second term is a small correction due to track cant and the third accounts for the effect of the height of the wagon centroid above the roll centre, adjusted for angular deflection of the wagon. These contact forces are for steady state or quasistatic conditions irrespective of roughness profile. In order to evaluate the slip conditions of each wheel for a given speed, the steady state cornering position of the bogie must be located. For this purpose, Figure 4 defines the bogie at zero yaw angle and angles of attack of the wheels.

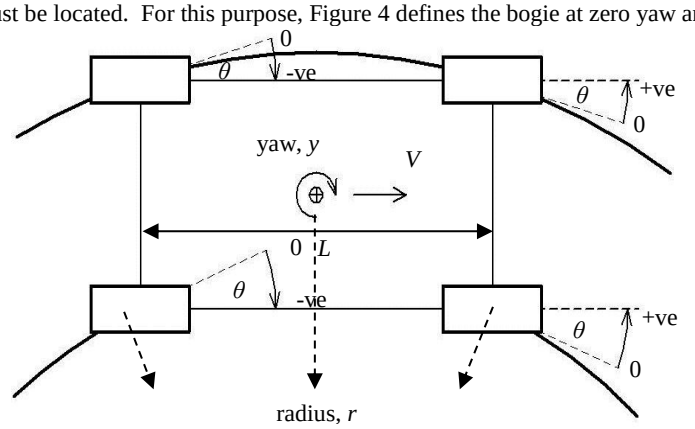

Figure 4 – Wheel angles of attack at zero bogie yaw, measured from the rail tangent to the wheel tangent

The traction forces were calculated based on a bogie yaw angle used to find angles of attack of each of the four wheels. With angles of attack and tangential velocity of the train known, the slip ratio on each wheel defined as,

$$\xi_i = \sin(-\theta_i(y)), \quad (11)$$

where the yaw angle of the bogie *y* determines the angle of attacks of each wheel θ_i according to the geometry of the (rigid) bogie on the curve as shown in Figure 4. This simplified analysis assumes large radius curves. The effect of flanging, conicity and train-related yaw torques in sharper curves would complicate this analysis requiring full wheel-rail profiles and complex kinematics of the bogie/train. Steady state cornering conditions are reached when the sum of lateral tractions, induced by these angles of attack via Equations (3), (4) with substitutions from Equations (9) and (10), balance the centripetal and gravitational force components in the direction perpendicular to the normal of the rails, as,

$$\sum Q_i(\xi, V) = m_t V^2 / [r\cos\beta] - m_t g \tan\beta \quad (12)$$

Longitudinal traction has been neglected by the current model which assumes that the mechanism of corrugations is via lateral traction variations interacting with vertical dynamics. This assumption is tested in the results section using a more complex 3D model as described in [17]. Since the angles of attack on the high and low rails, across a given wheelset, are approximately equal, most of the lateral traction forces will be provided by the wheel on the rail experiencing higher normal force. This will be the high rail on an under-canted corner and the low rail on an over-canted corner. The cant angle and velocity also play an important role in determining the required traction forces to navigate the corner. If the track is cant deficient for the given speed then the required sum of traction forces on the wheels will be positive (i.e. inwards) to counteract the centrifugal force. Assuming there is no flanging (i.e. the curve radius ~> 600 to 1000 m see [16]), increasing cant deficiency (i.e. unbalanced centrifugal force/speed) will decrease positive angles of attack on the leading wheelset and increase (the magnitude of) negative angles of attack on the trailing wheelset causing the bogie to have a positive yaw angle (turn into the curve). The opposite will occur if the track is over-canted for the given speed. It is noted that the effect of flanging, conicity and train-related yaw torques in sharper curves would complicate this analysis. The behaviour of the nonlinear bogie cornering model described by equations (2-12) was confirmed via benchmarking against Wickens [16] (chapter 4.4, page 117), simplified linear model for a two axle vehicle on large radius curves using Kalker's linear creep model [17] as detailed in Appendix B. The results concurred for small (linear variations) cant deficiencies as expected. Further discussion of the effects of uncertainties in curving conditions on corrugation growth results is provided in Appendix C.

In the presence of an oscillating normal force, the amplitude of oscillation in frictional power will be determined by the variation in creep $\Delta\xi$ which is driven by the variation in normal force amplitude, ΔP, such that,

$$\Delta P_{fric} = Q_i(\xi, V)V\Delta\xi = P_{fric}\Delta\xi / \xi_0 = P_{fric}C_{\xi P}\Delta P / P_0 \quad (13)$$

where $C_{\xi P}$ is the sensitivity of lateral creep to normal force fluctuations. The creep sensitivity was determined by calculating the partial differential of the creep curve given in Equation (3) for each set of cornering conditions. At creep ratios below critical, it can be assumed that the traction ratio remains constant with creep and the partial differential can be simplified to,

$$\frac{\partial\xi / \xi}{\partial P / P_0} = C_{\xi P}(\xi) = \frac{2 - \xi/\xi_c}{3(1 - \xi/\xi_c)^2} \quad (14)$$

Above critical slip, the traction ratio is not a closed form solution so a numerical finite difference approximation for solution to Equations (2), (4) and (5) was used.

2.3 Wear process (III)

Variation in wear may be calculated using the friction wear hypothesis that it is proportional to variations in frictional power. This means that variation in frictional power, when multiplied with an experimental wear coefficient, k_0 [18] gives the variation in rate of mass removal from the surface of the profile. Hence a relationship for the equivalent vertical depth of wear variation from the track surface, ΔZ, may be expressed as a function of the contact patch width, b, the material density, ρ, and the train velocity, v, as,

$$\Delta Z = k_0 \Delta P_{fric} / [2b\rho V] . \tag{15}$$

2.4 Corrugation growth over multiple passes with speed variation (IV)

Equations (1) to (15) define the models required to describe interactions between vibrational dynamics I, contact mechanics II and wear dynamics III of the bogie cornering corrugation mechanism shown in *Figure 2*. The corrugation growth feedback loop is closed when the change in profile height for each pass, ΔZ_n, is added to the existing profile, Z_n, to become the input profile for the next pass, Z_{n+1}. A single wheel pass transfer function can be created by multiplying each of the major steps in the corrugation growth feedback diagram of *Figure 2* and Equations (13) and (15) may be substituted into the resulting transfer function to obtain,

$$\frac{Z_{n+1}}{Z_n} = 1 + \frac{\Delta Z_n}{Z_n} = 1 + \frac{\Delta P}{Z_n}\frac{\Delta P_{fric}}{\Delta P}\frac{\Delta Z_n}{\Delta P_{fric}} , \tag{16}$$

$$\frac{Z_{n+1}}{Z_n} = 1 + K_b \frac{\Delta P}{k_c Z_n(\omega)} , \tag{17}$$

$$\text{where } K_b = \frac{k_c \Delta z_0 C_{\xi P}}{P_0} \tag{18}$$

$$\text{and } \Delta z_0 = \frac{k_0 Q \xi}{2b\rho} . \tag{19}$$

Hence corrugation growth may be predicted using Equations (17–19), which can be solved with substitutions from Equations (1), (2), (7), (9), (11) and (14) once the steady state cornering creeps and traction ratios are solved using Equations (2) to (12). It's important to consider here that conditions alternate between each successive wheelset pass as every bogie will have a leading and trailing wheelset, each under different steady state cornering conditions. A growth rate for a single equivalent wheel pass may be calculated based on an averaging of a full bogie pass as,

$$\frac{Z_{n+1}}{Z_n} = \sqrt{\frac{Z_{n+2}}{Z_n}} = K_{b/eq}\frac{\Delta P}{k_c Z_n(\omega)} + 1 \tag{20}$$

$$\text{where } K_{b/eq} = \frac{\left(K_{b(n\to n+1)} + K_{b(n+1\to n+2)}\right)}{2} . \tag{21}$$

At growth rates much less than one, the equivalent wear sensitivity $K_{b/eq}$ is simply the average of those of the leading and trailing wheel set of the bogie. The growth spectrum is fixed in wavelength or spatial frequency, so for a single wheel pass it is sufficient to leave it in terms of frequency, ω. When multiple wheel passes at varying speeds are considered, this frequency must be broken down to a ratio of speed to fixed wavelength, λ. When a probabilistic speed distribution, $p(V)$ is introduced [7], the growth rate of corrugation for a single equivalent wheelset pass then becomes,

$$G_r = \frac{Z_{n+1}}{Z_n} - 1 = \exp\int_{-\infty}^{\infty} \ln\left| K_{b/eq}(V)\frac{\Delta P}{k_c Z_n(V/\lambda)} + 1 \right| p(V)dV - 1 . \tag{22}$$

The growth rate function returns a spectrum in the wavelength domain. Therefore growth rate of the dominant wavelength of corrugation will be the maximum of this function across all wavelengths.

2.5 Probabilistic passing speed

In order to investigate the effects of speed distribution asymmetry on growth rate, a triangular probability density function was used. Two constraint cases were defined as being constant average with constant standard deviation, and constant average with constant domain width. Limits of statistical mode were chosen as full right angled left and right skewed curves and domain extremes were calculated to maintain the defined constraint cases. *Figure 5* shows a generic triangular skewed probabilistic distribution of speed, $p(V)$, over many vehicle passages with labels of domain limits, $V_{\min}$ and $V_{\max}$, mode, V_m and maximum height, defined by Equations (24) and (25).

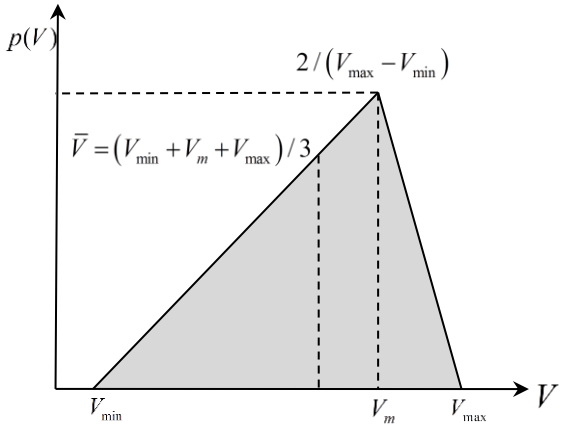

Figure 5 – Skewed triangular speed distribution curve used in the simulation (negative skewness i.e. high speed bias is depicted)

$$p(V) = 2(V - V_{\min})/[(V_{\max} - V_{\min})(V_m - V_{\min})] \qquad \text{If } V \le V_m, \tag{24}$$

$$p(V) = -2(V - V_{\min})/[(V_{\max} - V_{\min})(V_{\max} - V_m)] \qquad \text{If } V > V_m, \tag{25}$$

Referring to *Figure 5* and Equations (24) and (25), the equations of domain limits for each chosen statistical mode based on the pre-determined average, $\bar{V}$ and either the standard deviation, σ, or domain width, V_W are given by,

$$V_{\min,\max} = \frac{3\bar{V} - V_m}{2} \mp \frac{\sqrt{-3V_m^2 + 6\bar{V} \cdot V_m - 3\bar{V}^2 + 24\sigma^2)}}{2} = \frac{3\bar{V} - V_m}{2} \mp V_W / 2\,, \tag{26,27}$$

$$V_W = V_{\max} - V_{\min} \tag{28}$$

The standard skewness is defined as the second moment of a data set about the mean and is used as a standard measure of statistical spread asymmetry. For continuous distributions like the ones above, this can be evaluated as an integral of the distribution function, *p(V)*. For the triangular distributions used, this is given by,

$$S = \sum_{i=1}^{N} \left(V_i - \bar{V}\right)^3 \Big/ [(N-1)\sigma^3] = \frac{\sqrt{2}\left(V_{\min} + V_{\max} - 2V_m\right)\left(2V_{\min} - V_{\max} - V_m\right)\left(V_{\min} - 2V_{\max} - V_m\right)}{\left(V_{\min}^2 + V_{\max}^2 + V_m^2 - V_{\min}V_{\max} - V_{\min}V_m - V_{\max}V_m\right)^{3/2}}. \tag{29}$$

Twenty-five different, evenly spaced statistical modes were chosen between the domain limits for both fixed domain width and fixed standard deviation and 101 speeds were integrated within the domain of each associated distribution curve. All sets maintain an average of 90 km h^{-1} with the fixed standard deviation curves given a 15% standard deviation and fixed domain widths given a nominal width equal to the symmetric fixed standard deviation curve (i.e. S = 0). *Figure 6* a) shows a selection of five speed distribution curves for fixed standard deviation and b) for fixed domain width.

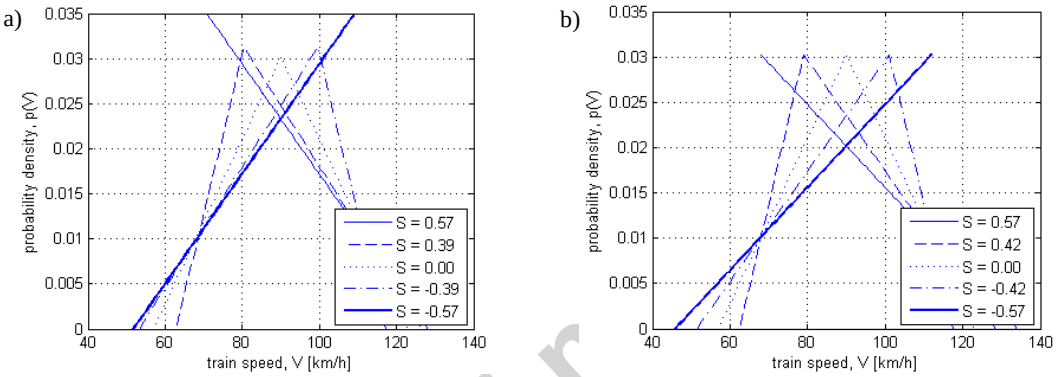

Figure 6 – Simulated a) fixed standard deviation and b) fixed width speed distribution curves

The fixed standard deviation curves experience a reduction in the domain width at the upper and lower limits of standard skewness and conversely, the fixed width curves have a higher standard deviation at the upper and lower limits of standard skewness.

3. RESULTS

Simulation parameters were chosen to represent a generic suburban site in Queensland (see Appendix D). These sites typically have ballasted track (700 mm crushed basalt) consisting of 50 kg m^{-1} rail (AS1085.1-1995) on Austrak M220 narrow gauge mono block concrete sleepers (~272 kg) spaced at approximately 0.66 m with Pandrol fist fasteners and rubber rail pads. The traffic is composed of 3 and 6 carriage electrical multiple unit (IMU/SMU) trains travelling at an average of 90 km h^{-1} with a standard deviation of 15%. The conditions simulated were of a curve with a 1000 m radius, track gauge of 1.067 m and a 55 mm cant yielding a 12.8 mm cant deficiency for the average speed of 90 km h^{-1}. The bogie has a wheelbase of 2.5 m and carries one half the mass of one loaded passenger wagon, 8818 kg above the wagon's geometric roll centre plus its own mass of 2271 kg. Dry contact conditions are assumed with a coefficient of friction of 0.4 at full sliding and 0.3 at high slip. For each speed within the domain of the chosen distribution curves, the steady state bogie yaw angle and wheel angles of attack were obtained by numerically solving Equation (12) with substitutions from (2) to (11). The wear sensitivity to contact force variation was then calculated using Equation (15) and the normal force variation due to an input profile was found for all frequencies using (1). The single pass growth rate was then calculated for each speed using Equation (20) with substitutions from Equations (18), (19) and (21) and substituted along with Equations (24) and (25) for the distribution function into Equation (22) to find the equivalent single pass growth rate for each distribution shape. To obtain confidence in the model, the corrugation growth rates under constant speed were compared with the more sophisticated (and computationally expensive) cornering model of Daniel et. al. [19]. In this case, an initial random track longitudinal profile was used. The comparison modelling predictions from Daniel et. al. [19] are valid for excitation up to 1000Hz (see [19]) and only excitations in this range are used.

The growth rate function, Equation (22), was integrated numerically with each given speed distribution shape as a function of corrugation wavelength. The maxima in the frequency domain were then used to evaluate the dominant growth rate. The numerical integration was performed via the trapezoidal rule with 100 speeds spread evenly across the distribution domain. A 41% reduction in maximum corrugation growth rate was observed with the 15% standard deviation distributed passing speed compared to the single pass corrugation growth rate at the mean speed. The numerical computation was performed on an Intel (R) Core 2 Duo 1.73 GHz CPU with 2 GB of RAM running a Windows XP Operating System and it took 170 s to complete 25 distribution shapes. In order to fully understand the contribution of cornering effects and skewness of speed distribution on corrugation growth, firstly corrugation

growth over a single pass is investigated to observe how varying speed can alter the critical parameters for corrugation growth under curving/cornering. Finally the combined effects of cornering conditions and skewness on corrugation growth rate are presented.

3.1 Isolated effects of speed on corrugation growth (no skewness)

To fully understand the effects of altering the speed distribution skewness, it's necessary to understand the relationship between corrugation growth rate and train speed for a single bogie pass. Since the cant angle, β, is small, the dominating effect of speed is the increase in tipping torque caused by the centrifugal force induced at the mass centroid. This will result in increasing normal force on the high rail approximately proportionally to velocity squared and a reduction in normal force on the low rail by the same amount depending on the wagon roll, β. *Figure 7* confirms these effects of speed on the high and low rail normal forces both with and without the inclusion of wagon roll in the calculation process.

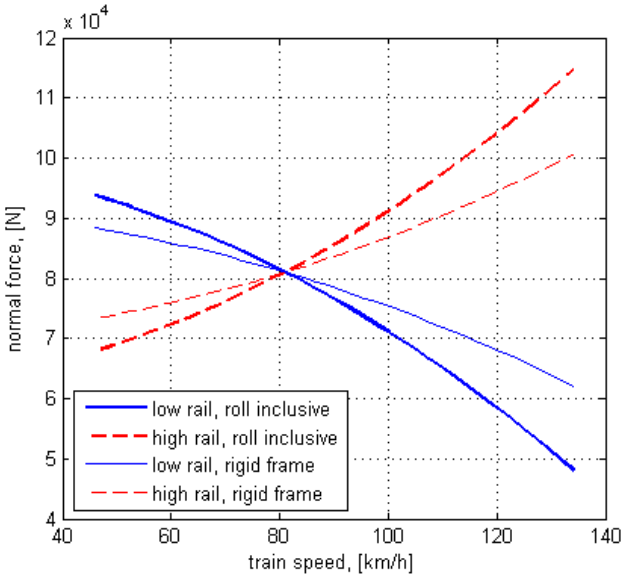

Figure 7 - Normal force on rails with changing speed

The results highlight the substantial effect of speed on normal force, that is enhanced by wagon roll, and in turn affects the corrugation growth rate. The growth rate over multiple passes will be the geometric mean of the growth rate for all speeds. Therefore, if particular speeds are prone to higher growth for a single pass, a higher probability density at this speed will result in a higher overall growth rate. *Figure 8* shows a) the maximum corrugation growth, normalised to its value at the neutral cornering speed, across all wavelengths, for a single wheel pass, as a function of speed and b) steady normal force wear and creep sensitivity parameters as a function of normalised speed with respect to the neutral cornering speed. The neutral curving/cornering speed is the speed under which the cant neutralizes the centrifugal force experienced by the cornering train.

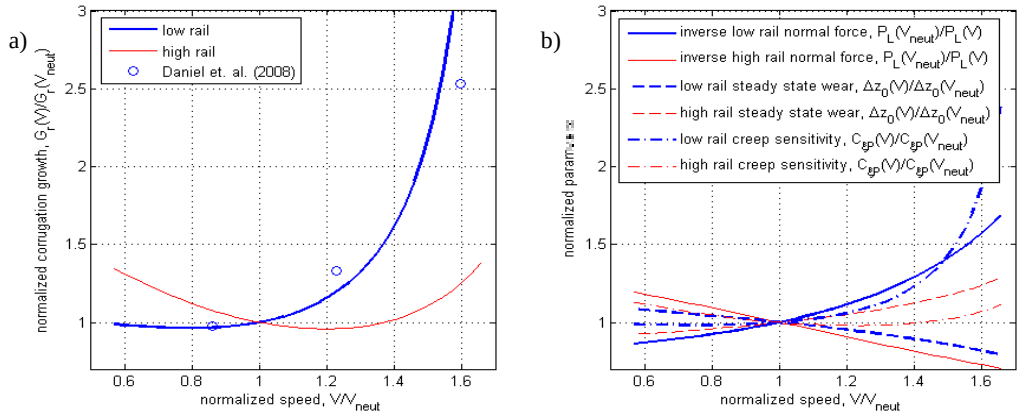

Figure 8 – Speed dependence of a) Corrugation growth rate and b) critical parameters affecting growth, normalized to neutral cornering conditions over a single bogie pass (average contribution from front and back wheels).

Figure 8 highlights that the normal forces, creep sensitivities and steady state wear on both front and back wheels and high and low rails are equal at the neutral cornering speed. The present efficient cornering model compares well with the multi degree of freedom numerical cornering modelling predictions from Daniel et. al. [19] (that has been validated with field measurements in [7]) with less than 14% error in relative changes in corrugation growth rate with speed as long as transient effects of sleeper spacing were ignored. It is noted that the amplitude of corrugations varies by 10% or so from one simulation to the next, due to a varied response to the initial random profile on the track. Corrugations of long pitches (>60mm) were found to be determined by the unsprung wheelset mass bouncing on the vertical receptance of the track. This mechanism is the same as that found using previous field validated predictions of corrugations in a curve described in [7,20]. From *Figure 8*a), the corrugation growth on the low rail increases substantially with train speed at a rate approximately proportional to the square of the normalised speed when speed is close to neutral, but increases much more rapidly at speeds far above neutral. This appears to be consistent with predicted increases in centrifugal tipping torque on the cornering vehicle and hence changes in normal contact forces with speed (see Equations (9) and (10)). To provide

more insight into this, the critical growth parameters in Equations (17–19) that change with normalised speed are plotted in *Figure 8*b). In particular, referring to the low rail results in *Figure 8*b), the inverse steady state normal force on the low rail, $1/P_L$, increases proportionally to the inverse square of the train speed,V, due to an increase in centrifugal tipping torque. In addition, the steady state wear, Δz_0, decreases proportionally to the normal force raised to the power of two thirds, according to Equation (19), as traction is proportional to normal force and contact patch width, *b*, is proportional to the cube root of normal force, while the lateral creep average over the bogie remains approximately constant. Hence referring to Equation (18), decreases in P_L and Δz_0 cause a combined increase in wear sensitivity to normal force with speed to the power of two thirds at close to neutral speeds but rapidly approaches infinite at much higher speeds due to the effect of creep sensitivity.

The creep sensitivity increases with speed due to a combined effect of reduction in critical creep proportional to the cube root of normal force as per Equation (5) and an increase in bogie yaw angle required to navigate the corner under higher centrifugal forces. These results are consistent with previous qualitative descriptions of trains in cornering on large radius corners (see Wickens, chapter 4) [16]. This effect is minimal at speeds close to neutral but will dominate the corrugation growth at much higher than neutral, as can be seen in *Figure 8*. The data plotted is averaged between the front and back wheels of a bogie, so the product of parameters for each rail in *Figure 8*b) will not match the corrugation growth in a), which is calculated via an average of wear sensitivity. If the curve/corner radius is significantly decreased, conicity effects must be considered to account for larger induced torque about the bogie yaw axis from opposing angles of attack between the front and back wheels on each rail. This will add a longitudinal wear element to corrugation growth which is expected to follow the same trends with speed as the lateral traction effects shown above. If the corner radius is small enough to initiate flange contact then multiple steady states of cornering may result, requiring complex stability analysis to perform further investigation into speed effects.

3.2 Combined effects of a skewed distribution and cornering on corrugation growth

It was of interest to investigate the spectrum of corrugation growth rates versus wavelength to identify the effect of skewness on roughness spectrum with the full effects of curving/cornering conditions included. *Figure 9* shows the growth rate (Z_{n+1}/Z_n-1) which has been normalised with respect to the maximum growth rate at constant vehicle speed, plotted against wavelength for a) fixed standard deviation and b) fixed domain width in speed. Normalised values above zero indicate corrugation growth.

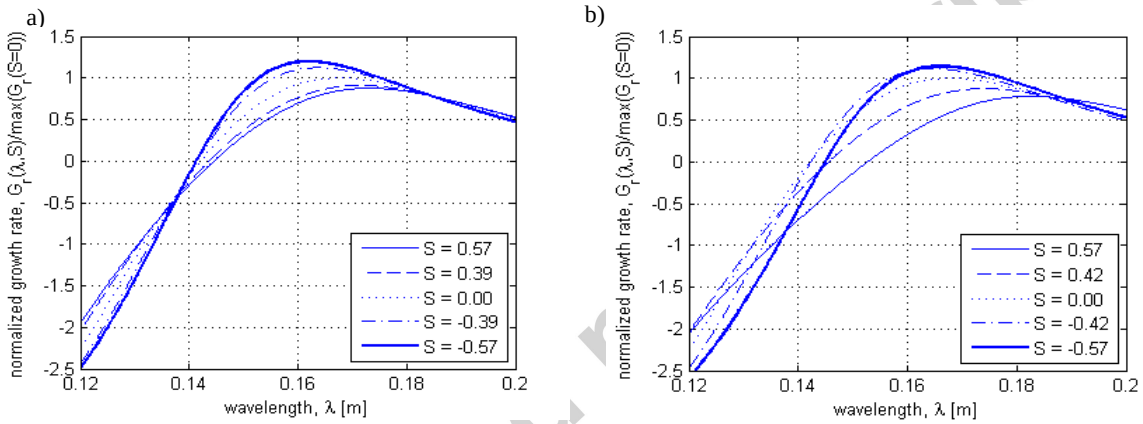

Figure 9 – Normalized corrugation growth rate on the low rail as a function of wavelength for five tested a) fixed standard deviation distribution curves and b) fixed width distribution curves

Note that a negative skewness indicates skew or a longer tail to the left and higher probability density for high speed and the opposite for positive skewness. By inspection of *Figure 9* the growth rate of corrugation at the dominant wavelength decreases and the dominant wavelength (approximately 165mm for no skewness) slightly increases with higher skewness. The higher growth rate correlates to a slightly lower wavelength, opposite to what would be expected if the wavelength were simply being scaled linearly with the statistical mode in speed. It has been shown that corrugation control via speed control behaves similarly to increasing the damping on the corrugation forming peaks, lowering the dominant frequency along with the peak spectral density [20]. This is likely the effect seen here. *Figure 10* shows the direct comparison of maximum growth rate of corrugation to speed distribution skewness.

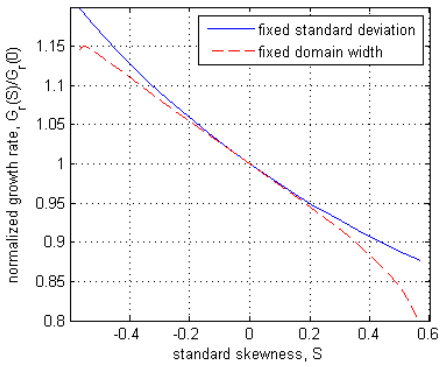

Figure 10 - Normalized corrugation growth rate change on the low rail with standard skewness for both fixed standard deviation and fixed width with speed-sensitive cornering conditions considered.

Note the nominal value $G_r(0)$ of the normalised corrugation growth rate reduction represents a decrease in the uncontrolled corrugation growth rate of 41% due to a symmetric distribution in speed. By inspection of *Figure 10*, it's apparent that in both the fixed width and fixed standard deviation cases that corrugation growth rate decreases with increasing skewness. This is most likely due to

the effects of cornering speed on the wear sensitivity parameter, K_b, as seen in *Figure 8*. When speed distribution is biased toward higher speed at a given site (i.e. skewness becomes more negative), a higher probability density will be apparent for speeds enhancing corrugation growth, primarily due to decreased lower rail normal forces with increased centrifugal tipping torque. Because of the influence that cornering effects have in this analysis, the sensitivity of these results will be increased with less stable cornering conditions such as tighter corner radii, more under-canted track and wider standard deviation in train passing speed.

According to the results in *Figure 10*, given a constant average train speed with fixed 15% standard deviation, the growth rate could be reduced by up to 12.3% from that of a symmetric speed distribution curve (41%) under the given site parameters. The minimum occurred when lower speeds were biased (i.e. positive standard skewness) while biasing towards higher speeds caused a potential increase in growth rate of 19.7%. It's expected that the magnitude of these changes due to asymmetry are proportional to the standard deviation. These results indicate that control of the asymmetry of speed distribution can have a substantial and increased effect under curving/cornering conditions as corner radius is reduced (under no flanging). Often a rail operator will prescribe a maximum or minimum speed on a given section of rail. This will sometimes require skewing the speed distribution curve to maintain a chosen average if corrugation control is attempted through increasing the speed variance. If a minimum train speed is dictated, the widest standard deviation is obtained for a given average when the speed distribution is positively skewed. Conversely, when a maximum speed limit is enforced, a distribution curve negatively skewed will result in the widest variance. This presents a problem in that the analysis presented in this paper shows that skewing the distribution curve in this manner can increase rail corrugation growth. For this reason, the effects of a skewed speed distribution should be considered before corrugation control via speed variance increase is employed at any given site.

4. CONCLUSIONS

An existing frequency domain corrugation growth model was modified to investigate the effects of an asymmetric speed distribution on the maximum growth rate for trains in cornering. The model included simplified quasistatic bogie/wagon cornering dynamics to navigate large radius corners including the effects of weight transfer between the high and low rail due to centrifugal tipping torque from cant deficiency. Curving/cornering results of traction and bogie yaw angle were benchmarked against a linearized cornering model presented in Wickens [16] and corrugation growth rate was benchmarked against modelling from Daniel et.al. [19] that was field validated in [7]. Flanging and coning effects were not considered.

Results showed that corrugation growth rate changed significantly in the presence of an asymmetric speed distribution as compared to a symmetric one. Under typical site parameters, a positive skew (higher distribution at lower speeds) in the speed distribution caused a decrease in corrugation growth while a negative skew (higher distribution at higher speeds) caused an increase. This was primarily caused by corrugation growth having a non-linear relationship with speed in cornering due to centrifugal forces as well as a less dominant spatial scaling effect between dynamic response frequency and corrugation wavelength spectra, independent of curving/cornering. These effects could be decreased significantly by decreasing the sensitivity of single pass growth rate to speed, achieved by either widening the curve/corner radius or decreasing the cant deficiency for the nominal speed. In particular, under the site parameters, an additional 12.3% reduction in corrugation growth rate due to speed variance could be achieved by skewing the speed distribution towards lower speeds from 41% reduction under a symmetric triangular speed distribution. This means that speed control via distribution skew manipulation without altering the average and standard deviation of train passing speed is feasible and could improve speed control-based corrugation mitigation schemes by up to 30%. It was also noted that if a maximum speed limit is enforced on a given site and corrugation mitigation is attempted via increased speed variance, the benefits of widening the distribution may be cancelled out either partially or fully by the effect of having a negative skewness (bias to higher speeds). In a worst case scenario, corrugation growth rate was shown to increase as much as 20% under the chosen site simulation parameters. This amounts to a 49% reduction in predicted effectiveness of speed control to reduce corrugation growth rate.

It should be noted that, in the current study, vehicle speed varies in a large interval (approximately between 40 km/h - 140 km/h) while the track and vehicle receptances are assumed to remain unchanged. It is possible that the spectral response of the coupled vehicle-track system could differ significantly with speed due to nonlinear effects on the receptances. The present bogie/wagon curving/cornering model also assumes there is no flanging which is typical for curves of radius ~> 600 to 1000 m (see [16]). Although the effect of flanging, conicity and train-related yaw torques in sharper curves would complicate this analysis, the model is still expected to provide guidance on the general behaviour of changes in corrugation growth rates due to changes in asymmetry of the speed distribution, as the normal load behavior is consistent. Also, although the present model has been benchmarked to corrugation growth of existing models that have been validated with field data, the effect of skewness of speed distribution has not been investigated in the laboratory or field; this is planned for future research.

ACKNOWLEDGEMENTS

The authors are grateful to the CRC for Rail Innovation (established and supported under the Australian Government's Cooperative Research Centres program) for the funding of this research as part of Project No. R3.158 Corrugation Control. The authors are also very grateful for the support and leadership of John Powell and researchers from Queensland Rail, Rail Infrastructure Corporation and the Australian Rail Track Corporation.

REFERENCES

[1] Sato, Y., Matsumoto, A. and Knothe, K., 2002, "Review on rail corrugation studies", *Wear* 253 pp. 130-139.
[2] Hempelmann, K. and Knothe, K., 1996, "An extended linear model for the prediction of short pitch corrugation", *Wear* 191 pp. 161-169.
[3] Müller, S., 2001, "Erratum to "A linear wheel-rail model to investigate stability and corrugation on straight track"", *Wear* 249 pp. 1117–1127.
[4] Wu, T.X. and Thompson, D.J., 2005, "An investigation into rail corrugation due to micro-slip under multiple wheel/rail interactions", *Wear* 258 pp. 1115-1125.
[5] Grassie, S.L. and Johnson, K.L., 1985, "Periodic microslip between a rolling wheel and a corrugated rail" *Wear* 101 pp. 291-309.
[6] Tassilly, E. and Vincent, N., 1991, "Rail corrugations: analytical model and field tests", *Wear* 144 pp. 163-178.
[7] Meehan, P.A., Bellette, P.A., Batten, R.D., Daniel, W.J.T., and Horwood, R.J., 2009, "A case study of wear-type rail corrugation prediction and control using speed variation", *Journal of Sound and Vibration* 325 pp. 85-105.
[8] Grassie, S., 2003, "Rail Corrugation: Advances in Measurement, Understanding and Treatment", *Proc. 6th International Conference on Contact Mechanics and Wear of Wheel/Rail Systems*, (CM2003), Sweden, June 10-13, 2003, pp. 11-15.
[9] Hoffmann, N.P. and Misol, M., 2007, "On the Role of Varying Normal Load and of Randomly Distributed Relative Velocities in the Wavelength Selection Process of Wear-Pattern Generation", *International Journal of Solids and Structures* 44 pp. 8718-8734.
[10] Bellette, P.A., Meehan, P.A., Daniel, W.J.T., 2008, "Effects of variable pass speed on wear-type corrugation growth", *Journal of Sound and Vibration* 314 pp. 616-634.
[11] Meehan, P.A. and Daniel, W.J.T., 2008, "Effects of wheel passing frequency on wear-type corrugations", *Wear* 265 pp. 1202-1211.
[12] Grassie, S.L. and Cox, S.J., 1984, "The dynamic response of railway track with flexible sleepers to high frequency vertical excitation", *Proc Instn Mech Engrs* 198D No 7.

[13] Johnson, K.L., 1987, Contact Mechanics, Cambridge University Press, Cambridge.
[14] Shen, Z.Y., Hendrick, J.K. and Elkins, J.A., 1993 "A comparison of alternative creep force models for rail vehicle dynamic analysis", *Proc. 8th IAVSD Symposium*, Cambridge, MA, 1993.
[15] Polach, O., 2003, "Creep forces in simulations of traction vehicles running on adhesion limit", *Proc. 6th International Conference on Contact Mechanics and Wear of Rail/Wheel Systems (CM2003)*, Gothenburg, Sweden, 2003.
[16] Wickens, A.H., 2003, Fundamentals of rail vehicle dynamics: guidance and stability, Swets & Zeitlinger Publishers, The Netherlands.
[17] Kalker, J. J., 1967, "On the rolling contact of two elastic bodies in the presence of dry friction", Thesis, Delft.
[18] Krause, H., and Poll, G., 1986, "Wear of Wheel-Rail surfaces", *Wear* 113 (1) pp. 103-122.
[19] Daniel, W.J.T., Horwood, R.J., Meehan, P.A., Wheatley, N, 2008, "Analysis of rail corrugation in cornering", *Wear* 265 pp. 1183-1192.
[20] Batten, R.D., Bellette, P.A., Meehan, P.A., Horwood, R.J., Daniel, W.J.T., 2010, "Field and theoretical investigation of the mechanism of corrugation wavelength fixation under speed variation", *Wear*, 271 1-2: 278-286.
[21] Kampfer, B.O., 2006, "New approach for predicting wheel profile wear", *Proc. 7th International Conference on Contact Mechanics and Wear of Rail/Wheel Systems (CM2006)*, Brisbane, Australia, September 24-26, 2006, pp. 675-680.
[22] Y. Suda, M. Hanawa, M. Okumuru and T. Iwasa, Study on rail corrugation in sharp curves of commuter line, Wear 253 (2002) 193-198.
[23] Eadie, D. T., Kalousek, J. and Chiddick, K. C., "The Role of Positive Friction (HPF) Modifier in the Control of Short Pitch Corrugations and Related Phenomenon", Wear 253 (2002), 185-192.
[24] PA Meehan, PA Bellette, RJ Horwood, "Does god play dice with corrugations?": Environmental effects on growth, Wear 314 (1), 254-260.

Appendix A – Modal track model

The track receptance used in the simulations performed was created using a 5-mode theoretical model. Typically there are only two dominant modes in the frequency range at which corrugation grows and three in the range chosen, so five modes are sufficient to over determine the system. The total track receptance as a function of frequency is given by the equation,

$$R_{vr}(\omega) = \sum_{m=1}^{5} R_m(\omega), \qquad \text{where } R_m(\omega) = 1/k_m - m_m(2\pi\omega)^2 + 2i\pi\omega c_m \quad \text{(A.1,2)}$$

The modal parameters used are given in the following table:

Table A.1. *Track model modal parameters*

Mode	Mass, m (kg)	Stiffness, k (kN m^{-1})	Damping, c (N s m^{-1})
1	380	162019	95504
2	40	2075046	400000
3	260	2739174	300000
4	100	1681623	26000
5	40	1021159	29000

The resultant receptance of these parameters is plotted in *Figure 11*.

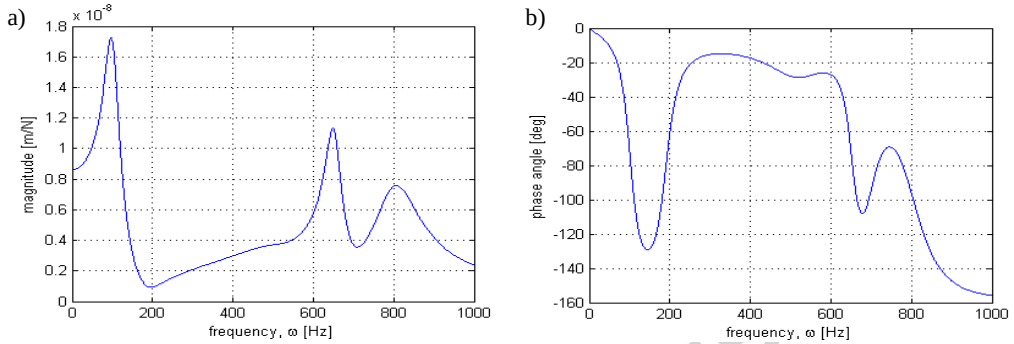

Figure 11 - Theoretical modal rail receptance a) magnitude and b) phase

The wheel receptance, R_{wv}, was assumed to be that of an unsprung mass mounted on the rail.

Appendix B – Comparison of results to Wickens [16]

The nonlinear bogie cornering model described in this paper was benchmarked against Wickens (chapter 4.4, page 117) [16], simplified linear model for a two axle vehicle on large radius curves using Kalker's linear creep model [17]. In particular, equations (2) to (12) were solved using an iterative routine to find the steady state bogie yaw, and subsequently all contact conditions Q_i, ξ_i and μ_i for each given speed, V. The simulations were performed under the conditions of corner radius of 1440 m, bogie length of 0.7452 m, train mass of 8000 kg per wheelset, and a nominal linearised lateral creep coefficient f_{22} = 7.69 MN at zero cant deficiency. In order to achieve this denominator of Equation (5) of nonlinear creep model was multiplied by a factor of 0.73. For the comparison of both models, traction and yaw were plotted as a function of cant deficiencies, Φ_D, defined as,

$$\Phi_D = \arcsin(v^2/rg) - \beta \qquad \text{(D.1)}$$

Figure 12 shows the direct comparison of results for change in a) traction from ideal cant conditions on each wheel/wheelset and b) bogie yaw, with increasing cant deficiency (ie increasing speed or decreasing curve radius).

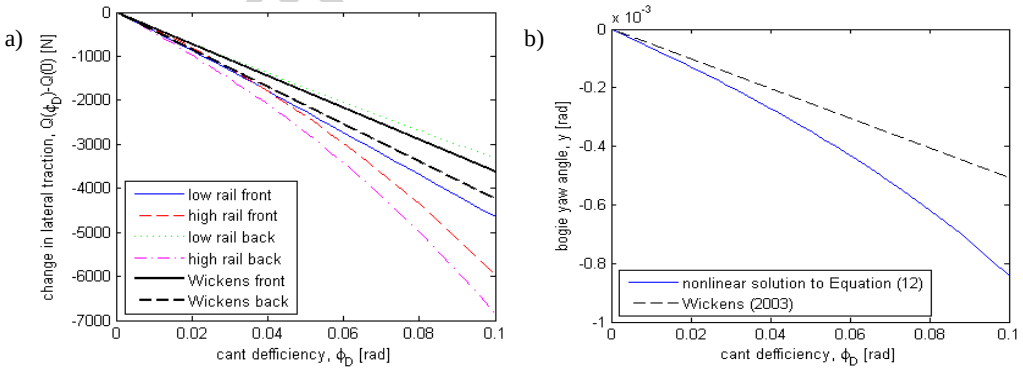

Figure 12 - Comparison of results to Wickens linear cornering model [17] a) lateral traction and b) bogie yaw

By inspection of *Figure 12* it is noted that total traction required to navigate the corner is underestimated by the linear cornering model at large cant deficiencies because the centrifugal forces are calculated using a small angle approximation. This reflects in an increased sum of lateral traction forces and a larger bogie yaw angle required to navigate the corner for the nonlinear model. In addition to this, the linear model does not consider the effects of centrifugal tipping torques causing transfer of weight from the low to the high rail with increased cant deficiency. This is reflected in diverging traction forces when comparing the high and low rail wheels on each. The negative changes in traction force on all four wheels correlate to decreasing positive angles of attack on the leading wheelset and increasing negative angles of attack on the trailing wheelset. Wickens predicts a linear relationship which closely resembles the nonlinear angles of attack predicted here [17].

Appendix C – Discussion of uncertainty in curving conditions on corrugation results.

The curving corrugation mechanism in this paper is based on the field and modelled behavior identified in [7] whereby cornering corrugations were shown to be associated with vertical vibrations interacting with lateral slip variations. Hence for computational efficiency (required in order to solve corrugation growth for a wide range of speeds), the model is focused on normal and lateral dynamic behavior only and the steady state effects of steering/conicity on this dynamic behavior is assumed to be small (for curve radii greater than 600-1000m). The benchmarking to the results of Wickens linear model for large radius curves (details in Appendix B) confirms this. In addition, a comparison with full bogie simulations with dynamic wear including the full wheel-rail profiles and multi-point contact/flanging (if required) has been performed using the more complex cornering model of Daniel et al [19] that has been validated to field measurements in [7] for corrugations in curves. These results, shown in figure 8 a), indicate that the effects of the simplifying assumptions on corrugation growth prediction for this case appear to be small.

The effect of uncertainties in curving behaviour on corrugation growth is not easy to determine but a guide may be provided in terms of the key growth parameters in equations (19) to (22). In particular, errors in nominal lateral traction and creep will directly change the steady state lateral wear and hence corrugation growth rate ie 10% changes in these parameters will cause 10% changes in corrugation growth rate. In addition, errors in nominal lateral traction and creep will also change the corrugation growth rate via changes in the sensitivity of lateral creep to normal force (related to the slope of the creep curve). The effect of these changes is not linear as is seen Figure 7 b) ie it can be large for conditions approaching saturated creep such as for high angle of attacks that may occur in sharp corners for the leading wheelset (particularly on the low rail that has a lower normal load due to centrifugal tipping at speeds above neutral see Fig 7). However the corrugation growth is approximately averaged over different wheelsets so this will tend to decrease the effect of errors. In addition, the effect of skewed distribution on growth rate is effectively averaged over multiple speeds which will also tend to decrease the error in results. Finally, this research is focused on changes in corrugation growth rate with respect to nominal corrugation growth conditions, so the effect of errors in steady state cornering conditions will only have indirect (second order) effects on the changes in corrugation growth rate due to asymmetry in speed distribution.

Appendix D - Simulation parameters and nomenclature

Constant value parameters stated, sequences are given ranges calculated variables have equation numbers.

a	half contact patch length (m)		Equation (6)
b	half contact patch width (m)		Equation (7)
B	creep equation exponent		0.02
C	track cant elevation (m)		0.055
C_{22}	Kalker coefficient		3.46
$C_{\bar{\varepsilon}P}$	creep sensitivity		Equation (14)
c_m	modal damping coefficient for mode, m (N s m^{-1})		Table 1
e	argument for complete elliptic integrals		Equation (B.1)
E	Young's modulus (Pa)		210×10^9
$\boldsymbol{E}$	complete elliptic integral of the second kind		
f_{22}	lateral creep coefficient (N), defined as $GabC_{22}$	[16]	6.79×10^6
F_1	contact patch eccentricity function		Equation (B.4)
g	acceleration of gravity (m s^{-2})		9.81
G	shear modulus (Pa)		80×10^9
G_r	corrugation growth rate		Equation (23)
h_b	height of bogie centre of mass from the rail (m)		0.25
h_{rc}	height of the geometric roll centre from the rail (m)		0.25
h_w	height of wagon centre of mass from the roll centre (m)		1.35
i	wheel number counted clockwise from front low		[1 – 4]
$\boldsymbol{K}$	complete elliptic integral of the first kind		
K_b	wear sensitivity to contact force variation		Equation (18)
$K_{b/eq}$	equivalent single wheel pass wear sensitivity for a bogie		Equation (21)
k_c	rail head contact stiffness (N m^{-1})		1×10^9
k_m	modal track stiffness for mode, m (N m^{-1})		Table 1
k_{roll}	rolling stiffness of the wagon at its roll centre		402000
k_0	wear coefficient [21]		2×10^{-9}
L	length of bogie between wheels (m)		2.5
m	track mode number		[1 – 5]
m_t	total train mass per wheelset (kg)		11089
m_b	mass of bogie per wheelset (kg)		2271
m_m	modal track mass for mode, m (kg)		Table 1
m_w	mass of wagon plus payload per wheelset (kg)		8818
m_u	unsprung mass per wheelset (kg)		970
n	wheel pass number		
N	statistical sample size		
p	probability density		Equations (24-25)
ΔP	normal force variance (N)		Equation (1)
ΔP_{fric}	frictional power variance (J s^{-1})		Equation (13)
P_H	normal force on high rail (N)		Equation (10)
P_L	normal force on low rail (N)		Equation (9)
P_0	normal force (N)		Equations (9-10)
Q	traction force (N)		Equations (3-4)
r	corner radius (m)		1000
R'	longitudinal relative radius of curvature of contact (m)		0.605
R''	transverse relative radius of curvature of contact (m)		2.400
R_m	modal track receptance for mode, m		Equation (A.2)
R_{rv}	vertical receptance of the rail		Equation (A.1)
R_{wv}	vertical receptance of the unsprung mass		Equation (A.3)

S	standard skewness	Equations (29)
V	train speed (m s^{-1})	[12.8 – 37.2]
$\bar{V}$	average train speed (m s^{-1})	25
V_{min}	lower domain limit of speed distribution (m s^{-1})	Equation (26)
V_m	speed distribution mode (m s^{-1})	
V_{max}	upper limit of speed distribution (m s^{-1})	Equation (27)
V_{neut}	neutral cornering speed (m s^{-1})	Equation (C.14)
V_w	speed distribution domain width (m s^{-1})	Equation (28)
w	track gauge (m)	1.067
x_b	horizontal distance of the bogie centroid from the high rail (m)	Equation (C.6)
x_{rc}	horizontal distance of the geometric roll centre from the high rail (m)	Equation (C.7)
y	yaw angle (rad)	
y_b	vertical distance of the bogie centroid from the high rail (m)	Equation (C.4)
y_{rc}	vertical distance of the geometric roll centre from the high rail (m)	Equation (C.5)
Δz_0	steady state wear depth (m)	Equation (19)
Z	profile height (m)	Equation (15)
α	wagon roll (rad)	Equation (C.3)
β	cant angle (rad)	0.052
θ	angle of attack (rad)	Equations (C.15-C.18)
λ	wavelength (m)	[0.06 – 0.3]
μ_i	traction ratio for wheel i	Equation (2)
μ_0	maximum coefficient of friction	0.4
μ_∞	coefficient of friction at infinite slip	0.3
ν	Poisson's ratio	0.3
ξ	creep	Equation (11)
ξ_c	critical creep	Equation (5)
ρ	density of rail steel (kg m^{-2})	7800
σ	speed standard deviation (m s^{-1})	5
Φ_D	cant deficiency (rad)	Equation (D.1)
ω	frequency (Hz)	[43 – 620]

HIGHLIGHTS

The highlights of this paper are:

1. Quantification of non-uniform speed distribution effects on corrugations in curves.
2. Validated efficient corrugation growth model with bogie curving dynamics.
3. Nonuniform speed distribution could add 30% to corrugation growth rate reduction.
4. Nonuniform speed distribution could reduce corrugation control performance by 50%.